Bjerknes forces between small cavitation bubbles in a strong acoustic field

R. Mettin,[1,*] I. Akhatov,[2,†] U. Parlitz,[1] C. D. Ohl,[1] and W. Lauterborn[1]
[1]*Drittes Physikalisches Institut, Universität Göttingen, Bürgerstraße 42-44, D-37073 Göttingen, Germany*
[2]*Ufa Branch of the Russian Academy of Sciences and Bashkir University, 6 Karl Marx Street, Ufa 450025, Russia*
(Received 10 March 1997)

The mutual interaction between small oscillating cavitation bubbles ($R_0<10$ μm) in a strong acoustic field ($P_a>1$ bar, $f=20$ kHz) is investigated numerically. We assume spherical symmetry and a coupling of the bubble oscillations. Our results show that the strength and even the directions of the resulting secondary Bjerknes forces differ considerably from predictions of the well-known linear theory. This is of immediate consequence for understanding and modeling structure formation processes in acoustic cavitation and multibubble sonoluminescence. [S1063-651X(97)01909-0]

PACS number(s): 47.55.Bx, 47.55.Dz, 47.55.Kf, 43.25.+y

INTRODUCTION

The mutual interaction between gas bubbles in an acoustic field is a well-known phenomenon which was discovered by Bjerknes [1]. There are two physical phenomena classified as Bjerknes forces: the attraction or repulsion of single bubbles at the pressure node or antinode of a stationary sound field, and the mutual attraction or repulsion of oscillating bubbles. However, both forces have a common cause—the radiation force set up by an acoustic pressure gradient. The force that influences the bubble due to the ''primary'' (external) sound field is called *primary Bjerknes force*, and the force between two bubbles due to the ''secondary'' sound fields emitted by other bubbles is called the *secondary Bjerknes force* [2].

The resonancelike oscillation behavior of small bubbles in strong acoustic fields [3–6] has been investigated recently with respect to its impact on the primary Bjerknes force [7,8]. In this paper, we address the effects of strong nonlinear radial oscillations on the mutual interaction of two bubbles due to the secondary Bjerknes force.

After the discovery by Bjerknes, the two types of force were investigated experimentally and theoretically by many authors [2,9–19]. The results concerning the secondary Bjerknes force are summarized in the following.

Weakly driven bubbles of fixed equilibrium radius R_0 show a maximum response at their linear resonance frequency $\hat{f}$. Accordingly, for a fixed driving frequency, the maximum response is shown by bubbles of linear resonance equilibrium radius $\hat{R}_0$. The relation between both is given by Minnaert's formula [20,5], which can be approximated for air bubbles in water under atmospheric pressure by $\hat{f}\hat{R}_0 \approx 3$ m/s. If the driving frequency lies between the two linear resonance frequencies of the individual bubbles, they will repel each other; otherwise an attractive force is present. However, this result is based on the assumption of *harmonically* oscillating spherical bubbles, which is valid only if the pressure amplitude of the acoustic field is very small and the spacing between the two bubbles is very large.

During the last years substantial progress has been achieved in the development of this theory. In Refs. [15] and [16] two coupled oscillating bubbles were considered in linear theory, and also for small distances. It was shown that the resonance frequencies of the two-bubble system will change as the bubbles approach each other, leading to a phase shift between the bubble oscillations which may, in turn, change the sign of the mutual interaction force. In Ref. [17] the multiple scattering of sound between the bubbles was taken into account, also in a linear framework. It was again shown that for bubbles which are larger than resonance size (i.e., whose linear resonance frequencies are smaller than the driving frequency) the attractive force can become a repulsive force if the bubbles come close to each other. The reason for this deviation from the standard linear theory is the fact that when the bubbles oscillate in phase their adjacent walls move against each other, producing an additional stiffness in the oscillations. This in turn causes the effective resonance frequencies of both bubbles to increase. When approaching, the effective resonance frequency of the smaller bubble first rises above the driving frequency and the attraction changes to repulsion.

Oguz and Prosperetti [18] investigated the interaction of two nonlinearly oscillating bubbles. They assumed that the distance between their centers is large so that the bubbles remain spherical at all times. The sizes of the bubbles considered have been of the order of 100 μm, the frequency of the external sound field has been taken comparable to the linear resonance frequency of the bubbles, and the amplitude of the driving pressure did not exceed 0.5 bar. For such a relatively small pressure amplitude the bubbles of that size oscillate just slightly nonlinearly, but without strong collapse. Therefore the compressibility of the liquid is negligible, and the approximation of an incompressible fluid has been used. It was shown that nonlinear effects can influence the interaction so strongly that the sign of the force changes compared with the prediction of the linear theory. In particular, the repulsion may also appear in the case of two bubbles driven *below* their linear resonance frequencies. This feature may be explained taking into account the first nonlinear resonance where the bubble oscillation contains a strong component at twice the driving frequency. The effect can be con-

*Electronic address: robert@physik3.gwdg.de
†Electronic address: iskander@ncan.bashkiria.su

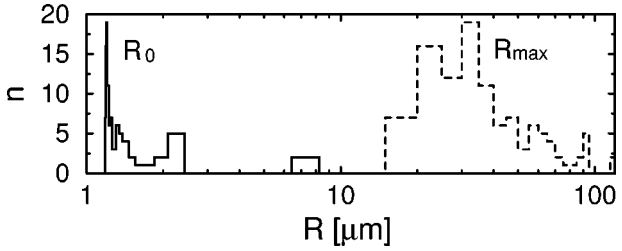

FIG. 1. Size distribution of cavitation bubbles in water. Dashed: bubble counts n vs measured (maximum) radius R_{max} (experimental values from Ref. [23]). Solid: recalculated equilibrium radii R_0.

sidered as a double-frequency driving, which might be below resonance for the smaller bubble and above resonance for the larger one.

A different approach was presented by Pelekasis and Tsamopoulos [19]. They investigated numerically the motion of two bubbles in an incompressible liquid induced by an oscillatory disturbance of the ambient pressure, taking into account the shape deviations of the bubbles from sphericity. If the driving frequency lies in the interval defined by the individual breathing-mode resonance frequencies, a repulsion of the bubbles is observed. Since the magnitude of the breathing-mode frequencies depends on the distance between the bubbles, the sign of the interaction force may change as the bubbles come closer to each other.

In our investigation of the mutual bubble interaction we consider coupled cavitating bubbles which remain spherical, and are therefore assumed to be not too close to each other. We suppose strong sound fields with driving pressure amplitudes P_a exceeding 1 bar, which is higher than the range considered in all papers cited above. Such fields with frequencies in the kHz range occur, for example, in multibubble sonoluminescence experiments [21]. The strong driving qualitatively changes the character of the bubble oscillations: if R_0 is larger than a certain value (''dynamical Blake threshold''), surface tension is exceeded by the driving pressure, and a significant expansion, followed by a violent collapse of the bubble, takes place during every cycle. The bubble wall's motion is strongly anharmonic, and the heavy collapse implies that damping by sound radiation should be taken into account when calculating the bubble radius evolution. The response curves (normalized maximum bubble radius vs the equilibrium radius) for this type of bubble oscillations were previously investigated [3,4] and used to analyze the rectified diffusion [6,22] and the primary Bjerknes force [8] acting on a bubble in a strong acoustic field.

The choice of the bubble sizes considered here is motivated by the experimental bubble size statistics of cavitating water under strong acoustic fields that is shown in Fig. 1 (dashed line). This distribution which is taken from Ref. [23], was measured at the phase of the sound field when a maximum bubble expansion occurs. It is peaked between 25 and 100 μm. The equilibrium radius distribution (solid line) was from these measured values using the response curves of a single bubble under strong forcing corresponding to the experimental setup in [23] ($P_a=1.5$ bar, $f=10.5$ kHz). It shows that the majority of the cavitating bubbles has an equilibrium radius R_0 below 10 μm. Thus in this paper we analyze the Bjerknes forces between small bubbles ($R_0<10$ μm) in a strong acoustic field ($P_a>1$ bar). The considered driving frequency $f=20$ kHz is always below the bubbles' linear resonance frequencies that lie above 300 kHz.

I. MATHEMATICAL MODEL

Let us consider two gas bubbles in a liquid driven by a stationary sound field of wavelength large compared with the radii of the bubbles and the distance between their centers. Thus both bubbles experience pressure oscillations of the same amplitude and phase. In the case when the spacing between the bubbles is large compared with their size, we may assume that the bubbles remain spherical for all time with radii $R_1(t)$ and $R_2(t)$, respectively. Furthermore, one can consider the motion of the liquid around the first oscillating bubble also to be spherically symmetric. In the vicinity of an oscillating bubble the incompressible liquid approximation is valid [24,25], and the velocity field $w_1(r,t)$ may be written in the form

$$w_1=\frac{R_1^2\dot{R}_1}{r^2}. \tag{1}$$

Here r is the radial coordinate, the dot denotes the time derivative, and the origin of the coordinate system coincides with the center of the first bubble.

To calculate the respective pressure field, the equation of liquid motion is used,

$$\rho\ \frac{\partial w_1}{\partial t}+\frac{\partial p_1}{\partial r}=0, \tag{2}$$

where ρ is the density of the liquid and p_1 is the pressure in the liquid emitted by the first bubble. We omitted the nonlinear convective term $w_1\partial w_1/\partial r$ in Eq. (2), because it is of the order of r^{-5} and therefore much smaller than the first term. Substitution of Eq. (1) into Eq. (2), and integration, yields the following formulas for the pressure gradient and the pressure:

$$\frac{\partial p_1}{\partial r}=-\frac{\rho}{r^2}\frac{d}{dt}\ (R_1^2\dot{R}_1),\quad p_1=\frac{\rho}{r}\frac{d}{dt}\ (R_1^2\dot{R}_1). \tag{3}$$

It should be noted that the influence of the first bubble on the second bubble is *twofold*. The *pressure gradient field* is the source of the Bjerknes force acting from the first bubble on the second, and the *pressure field* represents an additional driving pressure for the second bubble.

A bubble of volume $V_2=4\pi R_2^3/3$ in a liquid under a pressure gradient ∇p_1 experiences a force

$$\mathbf{F}_{12}=-V_2\nabla p_1. \tag{4}$$

Substituting Eq. (3) into Eq. (4), one obtains the force of the first bubble on the second one at distance d:

$$\mathbf{F}_{12}=-V_2\ \frac{\partial p_1}{\partial r}\bigg|_{r=d}\mathbf{e}_r=V_2\ \frac{\rho}{d^2}\frac{d}{dt}\ (R_1^2\dot{R}_1)\mathbf{e}_r$$

$$=\frac{\rho}{4\pi d^2}\ V_2\ \frac{d^2V_1}{dt^2}\ \mathbf{e}_r. \tag{5}$$

$V_1 = 4\pi R_1^3/3$ is the volume of the first bubble, and $\mathbf{e}_r$ denotes the radial unit vector.

If the bubble volumes vary periodically in time, the net force on the second bubble is the time average of $\mathbf{F}_{12}$ over one period. This net radiation force acting on a neighboring spherical bubble in a sound field is called the *secondary Bjerknes force* $\mathbf{F}_B$ [2]. Integrating Eq. (5) over a period of the volume oscillations and using partial integration, one obtains the known formula for the secondary Bjerknes force,

$$\mathbf{F}_B = \langle \mathbf{F}_{12} \rangle = -\frac{\rho}{4\pi d^2} \langle \dot{V}_1 \dot{V}_2 \rangle \mathbf{e}_r , \tag{6}$$

where $\langle\ \rangle$ denotes the time average.

We assume that the bubbles are driven by an external pressure $p_{\mathrm{ex}} = P_a \sin(2\pi f t)$. Further, we suppose that the bubbles are far enough apart that their pressure emissions have the effect of an additional external driving of their neighbor without distorting each other's sphericity. Thus the pressure p_1 generated by the first bubble adds to the sinusoidal driving p_{ex} of the second bubble.

For calculation of the bubble oscillations, we use the model of Keller and Miksis [26] with a series expansion of the retarded driving term [27,28]. Using p_1 from Eq. (3) and neglecting coupling terms of order $(R_i/d)(\dot{R}_j/c)$ and $(R_i/d)[(d^3/dt^3) R_j/c], i,j = 1,2$ leads to the equation of bubble 2:

$$\begin{aligned} &\left(1 - \frac{\dot{R}_2}{c}\right) R_2 \ddot{R}_2 + \left(\frac{3}{2} - \frac{\dot{R}_2}{2c}\right) \dot{R}_2^2 \\ &\quad = \frac{1}{\rho} \left(1 + \frac{\dot{R}_2}{c}\right) [p_{2w} - p_{\mathrm{stat}} - p_{\mathrm{ex}}] + \frac{R_2}{\rho c} \frac{d}{dt} [p_{2w} - p_{\mathrm{ex}}] \\ &\quad - \frac{1}{d} (2\dot{R}_1^2 R_1 + R_1^2 \dot{R}_1). \end{aligned} \tag{7}$$

Here, p_{2w} is the pressure in the liquid at the bubble wall. We omit vapor pressure terms and assume adiabatic compression of an ideal gas within the bubble, which yields

$$p_{2w} = \left(p_{\mathrm{stat}} + \frac{2\sigma}{R_{20}}\right) \left(\frac{R_{20}}{R_2}\right)^{3\gamma} - \frac{2\sigma}{R_2} - \frac{4\mu}{R_2} \dot{R}_2 . \tag{8}$$

R_{20} is the equilibrium radius of the second bubble, p_{stat} is the atmospheric static pressure, γ denotes the polytropic exponent, σ is the surface tension, and μ is the viscosity of the liquid.

It is straightforward to calculate that the influence of the pressure field of the second bubble on the first bubble is of the same form. Therefore, the equations for the oscillations of the first bubble coincide with Eqs. (7) and (8) for exchanged indices $1 \leftrightarrow 2$. Thus, to calculate the secondary Bjerknes force between two small gas bubbles in a strong acoustic field, one has to solve a coupled system of ordinary differential equations, consisting of Eqs. (7) and (8) and their versions with exchanged indices, and use the solution in the averaging procedure [Eq. (6)]. Furthermore, it turns out that the secondary Bjerknes forces of both bubbles are symmetric: $\langle \mathbf{F}_{21} \rangle = -\langle \mathbf{F}_{12} \rangle$ in the same coordinate system. A positive sign of $\langle \dot{V}_1 \dot{V}_2 \rangle$ means attraction, a negative sign repulsion.

Generally, there is a time delay $\tau \approx d/c$ between an oscillation of the first bubble and the action of the pressure p_1 on the second bubble at a distance d. For $d \approx 1$ mm, which is a typical distance of bubbles in structure formation [23], the delay time $\tau \approx 0.6\ \mu$s is in the range of only 1% of the driving period ($f = 20$ kHz, $T = 50\ \mu$s). Nevertheless, it might play an important role, because even a small time shift of the collapse can have a strong influence on the averaging [Eq. (6)]. The delay effect is not in the scope of this paper, and will be investigated elsewhere. We want to note, however, that the symmetry of the mutual forces is in general destroyed if a delay is taken into account.

II. NUMERICAL RESULTS

The calculations were carried out with atmospheric static pressure $P_{\mathrm{stat}} = 1$ bar and driving frequency $f = 20$ kHz. The other parameters were set to $c = 1500$ m/s, $\rho = 998$ kg/m^3, $\sigma = 0.0725$ N/m, $\mu = 10^{-3}$ kg/(m s), and $\gamma = 1.4$.

The average in Eq. (6) was calculated after transients had decayed. Almost all choices of R_1, R_2, P_a, and d in this paper led to bubble cycles of period 1, i.e., the period of the bubble oscillation equalled the driving period. Exceptions occurred only in a few cases with one or both of the equilibrium radii between 8 and 10 μm. Then the average was calculated with respect to the higher period which appeared. No chaotic oscillations [28] were detected in the considered parameter range.

For presentation of the results, the secondary Bjerknes force coefficient f_B is used, which we define as

$$f_B = \frac{\rho}{4\pi} \langle \dot{V}_1 \dot{V}_2 \rangle . \tag{9}$$

The force of one bubble on the other is found by dividing f_B by d^2. The sign of f_B indicates attraction ($f_B > 0$) or repulsion ($f_B < 0$) of the bubbles.

The main results are presented in Figs. 2 and 3, where the Bjerknes force coefficients f_B are shown in a grayscale coding in the R_{10}-R_{20} plane for different driving pressures and distances. For better visualization, the complete symmetric data are shown. In Fig. 2 the bubbles are uncoupled, i.e., a very large distance d is assumed. The white regions correspond to repulsive forces, darker areas to attraction between the bubbles. It can be seen that repulsive (white) stripes form which shift to smaller radii for increasing pressure. This phenomenon does not appear for weaker driving ($P_a < 1$ bar). For larger pressure, the following structure becomes more and more pronounced: a plateaulike region of strong attractive forces builds up at larger bubble sizes (dark square). It is separated from weak attractive regions (light gray) by the white stripes of repulsive forces.

In Fig. 3, the alteration is shown for approaching bubbles, i.e., for increasing influence of the coupling pressure field between them. The main structure is preserved: A separation into weak and strong attracting regions, accompanied by a large increase of f_B after the repulsive stripes, is still present. However, the regions of repulsive forces shrink. Additionally, for $P_a = 1.32$ bar [Figs. 3(c) and 3(d)], their borders

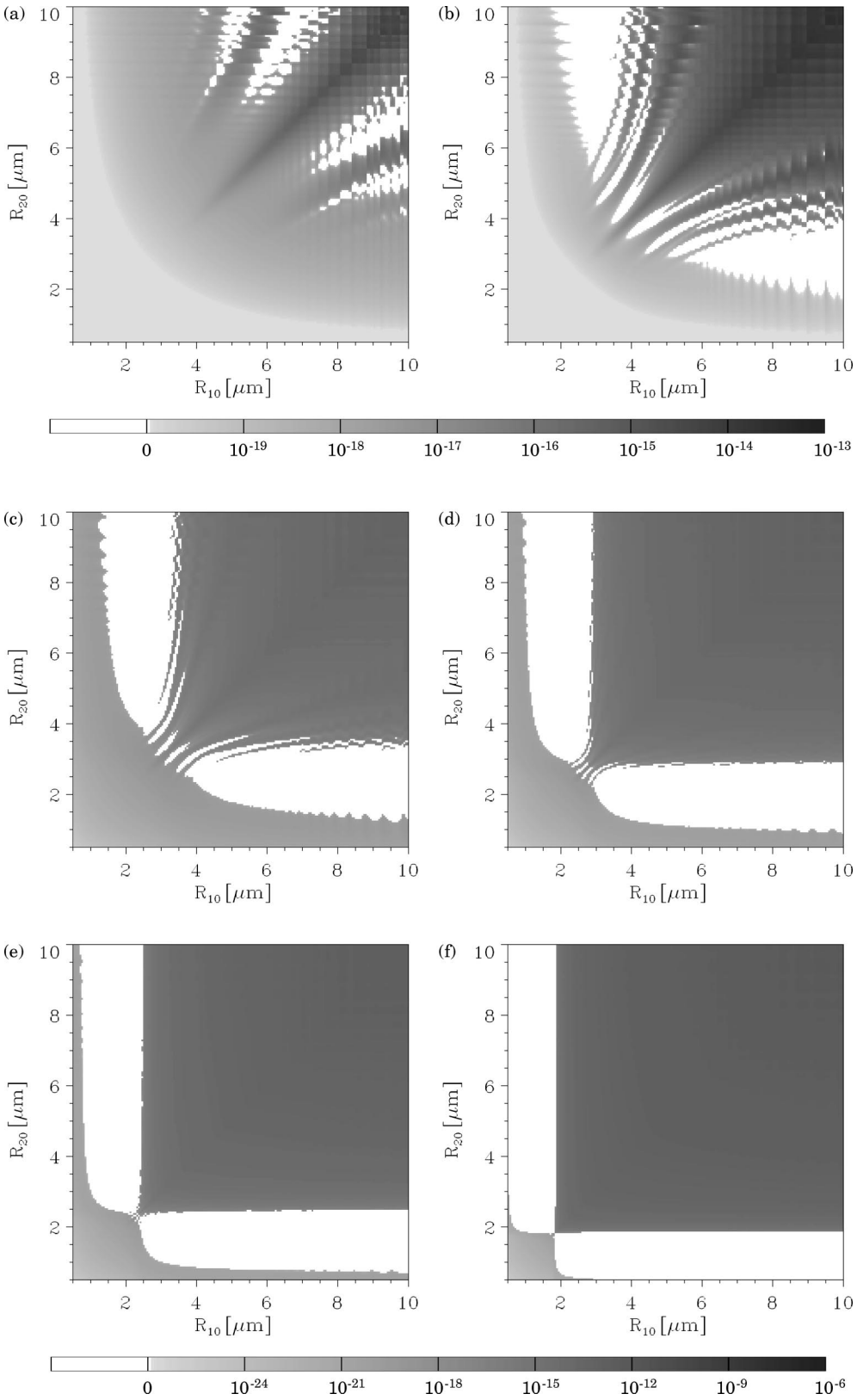

FIG. 2. Secondary Bjerknes force coefficient f_B in the R_{10}-R_{20} plane for uncoupled equations, i.e., for large bubble distance d. The planes are given for driving amplitudes $P_a = 1.04$ (a), 1.12 (b), 1.16 (c), 1.20 (d), 1.24 (e), and 1.32 bar (f). Repulsive forces (negative f_B) are represented by white areas. Attractive forces (positive f_B) are coded in gray scales according to the bars below the figures.

shift slightly to larger bubble sizes. Thus, for some bubble pairs, the approach leads to inversion of the secondary Bjerknes force (compare Fig. 5).

The findings result from the underlying resonancelike structure of the dynamical Blake threshold. For illustration, let us consider a section of Fig. 2(f), $P_a = 1.32$ bar, for a constant second bubble size of $R_{20} = 5$ μm. The corresponding main nonlinear resonance behavior of the first bubble

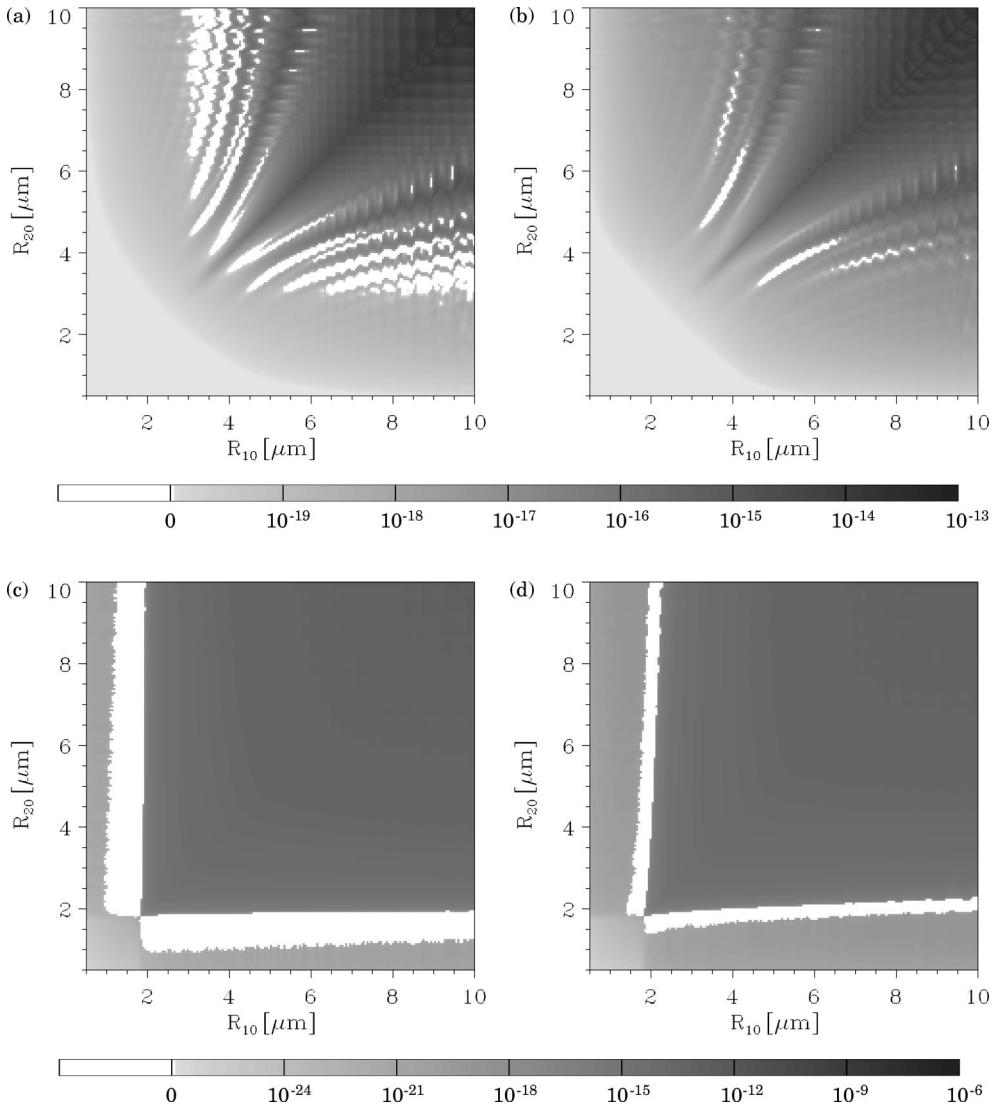

FIG. 3. Secondary Bjerknes force coefficient f_B in the R_{10}-R_{20} plane for coupled equations. Upper row: driving amplitude $P_a = 1.12$ bar, $d = 1$ mm (a), and $d = 0.2$ mm (b); lower row: $P_a = 1.32$ bar, $d = 1$ mm (c), and $d = 0.2$ mm (d). White area indicates negative f_B, positive values of f_B are coded in gray scales according to the bars below the figures.

together with the typical dependence of the Bjerknes force coefficient on R_{10} is shown in Fig. 4.

The normalized maximum radius of the first bubble, $R_{1\,\max}/R_{10}$, is plotted vs its equilibrium radius R_{10} in Fig. 4(a). The different curves are results for different distances of the second bubble. Both bubbles are exposed to the sound field amplitude of $P_a = 1.32$ bar. The uppermost curve is obtained for uncoupled equations (i.e., large distance). Bubbles smaller than about 2 μm oscillate with low amplitude and nearly sinusoidally, which is due to the surface tension. At about 2.5 μm a resonancelike maximum appears. The bubble enlarges by more than a factor of 12 during a strong nonlinear oscillation which shows a bouncing behavior with a violent collapse. For larger equilibrium radii, the ratio $R_{1\,\max}/R_{10}$ decreases, and a structure with smaller secondary resonance maxima evolves. These secondary resonances are the reason for the pattern of squares appearing at large radii in Figs. 2(a) and 2(b).

For a closer approach of the second bubble, the main maximum decreases and is shifted slightly to larger radii. The curve which denotes the response for a distance of $d = 0.1$ mm is dashed because the approaching bubble is already close to overlap with a $R_{10} = 10$ μm bubble during their maximum extensions, and the assumption of spherical bubbles is surely not fulfilled. (However, for bubbles of $R_{10} < 2$ μm, this distance can still be considered large.) The effect of the second bubble coming closer is obviously similar to a decreasing effective driving pressure (compare curves in Ref. [6], Fig. 2). This can be explained by a mutual hindrance of the oscillations, which is similar to coupled linear in-phase oscillations [15–17].

The magnitude of the Bjerknes force coefficient f_B is very sensitive to the bubbles' radii. If we suppose small oscillations ΔR_i around R_{i0}, $i = 1$ and 2, with $\Delta R_i/R_{i0} \approx$ const, we find a linear scaling between bubble wall velocity and equilibrium radius. Therefore, we can roughly estimate $\langle \dot{V}_1 \dot{V}_2 \rangle$ being proportional to $R_{10}^3 R_{20}^3$. This leads already in a linear approximation to a scaling over six orders of magnitude in the considered range of bubble equilibrium sizes. The jump in (dynamic) bubble size by a factor of about 10, caused by the indicated resonancelike effect, means an additional scal-

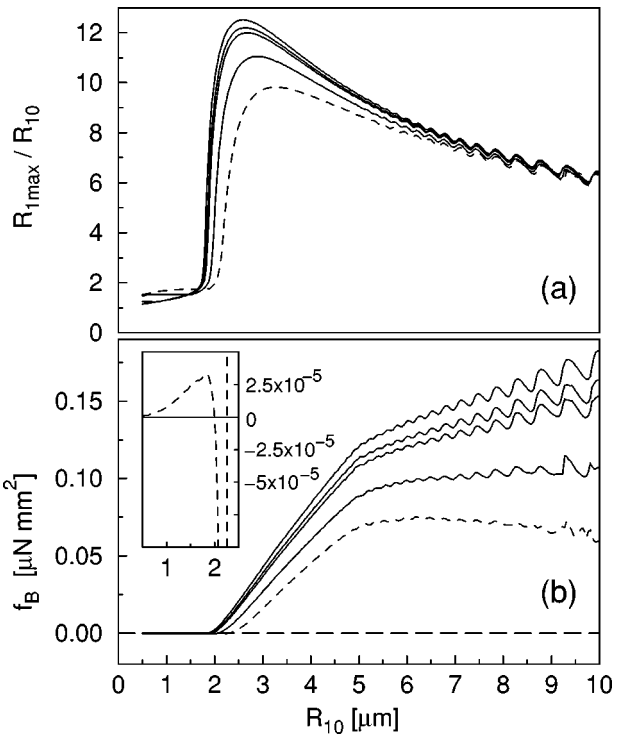

FIG. 4. Resonancelike response and secondary Bjerknes force for $P_a = 1.32$ bar. From the uppermost to the lowermost line, the results are given for a second bubble ($R_{20} = 5\ \mu$m) which is located at large d (uncoupled), $d = 1$, 0.6, 0.2 mm, 0.1 mm (dashed). (a) Normalized maximum radius $R_{1\,\max}/R_{10}$ vs the first bubble's equilibrium radius R_{10}. (b) Bjerknes force coefficient f_B. Inset: magnification of f_B for $d = 0.1$ mm.

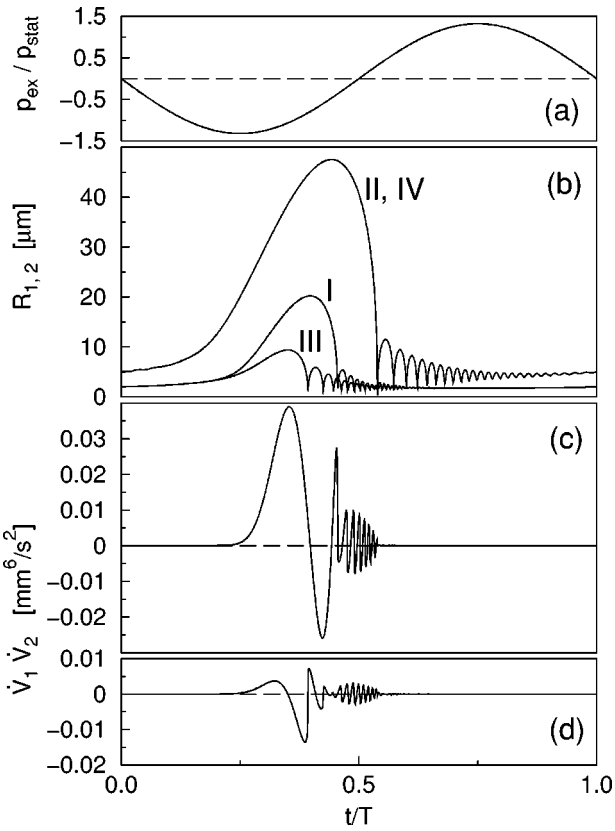

FIG. 5. Normalized driving pressure p_{ex}/p_{stat} (a), and bubble radii $R_{1,2}$ (b) vs normalized time t/T during one driving period ($P_a = 1.32$ bar, $R_{10} = 2\ \mu$m, and $R_{20} = 5\ \mu$m). Curves I and II in (b) correspond to R_1 and R_2 for the uncoupled case (d large). Curves III and IV indicate R_1 and R_2 for $d = 0.2$ mm. The time-dependent part of the average in Eq. (6), $\dot{V}_1\dot{V}_2$, is shown for the uncoupled case [(c), $f_B > 0$] and for $d = 0.2$ mm [(d), $f_B < 0$].

ing of six orders of magnitude. Indeed, Fig. 4(b) shows a strong increase of f_B at the dynamical Blake threshold. As the second bubble remains unchanged in this figure, the jump amounts for a factor of about 10^3.

It is an important result of Figs. 2 and 3 that the mutual bubble forces are not always attracting, although the driving frequency is always much smaller than the linear resonance frequency. The dynamical Blake threshold is accompanied by some phase shift of the bubble radius maxima and minima, similar to a phase shift at a linear type of resonance. Therefore, we find some range of bubble sizes with repelling forces. This region contains bubble pairs with one bubble smaller (but not too small) and the other bubble larger than the nonlinear resonance size. The enlargement in Fig. 4(b) magnifies the dashed curve ($d = 0.1$ mm) in this region. The typical structure, which is shown also by the other curves, has two zero crossings left to the resonance maximum, bracketing the repelling region.

An approach of the second bubble has a decreasing effect on the Bjerknes force coefficient, as the oscillations become less strong. The repelling regions shift slightly to larger radii and shrink, i.e., the zero crossing points become closer [which cannot be seen in Fig. 4(b), but in the plane view of Figs. 3(c) and 3(d)]. The influence of the pressure field coupling is illustrated in Fig. 5, where the radius evolution in time is shown for two bubbles of sizes $R_{10} = 2\ \mu$m and $R_{20} = 5\ \mu$m. For $P_a = 1.32$ bar this bubble pair is close to the border of the repelling region in the R_{10}-R_{20} plane [cf. Figs. 2(f), 3(c), and 3(d)]. If the bubbles are far apart, oscillations are uncoupled and we obtain the curves I and II in Fig. 5(b) for bubbles 1 and 2, respectively. Averaging of $\dot{V}_1\dot{V}_2$ [Fig. 5(c)] yields a positive Bjerknes force coefficient $f_B = 2.4\times10^{-3}\ \mu\text{N}\times\text{mm}^2$, and thus bubbles are attracting each other. If the bubbles approach to a distance $d = 0.2$ mm, they oscillate as indicated by curves III and IV in Fig. 5(b). Curve IV seems identical to curve II, since the larger bubble's behavior hardly changes, but the smaller bubble is less enlarged and collapses earlier. The function $\dot{V}_1\dot{V}_2$ is altered according to Fig. 5(d), and averaging results in a negative $f_B = -6.7\times10^{-5}\ \mu\text{N}\times\text{mm}^2$. In this case, the pressure field coupling changes the effect of the secondary Bjerknes force from attraction to repulsion if the bubbles come close to each other. This implies the existence of a stable equilibrium distance between both strongly oscillating bubbles. However, for most combinations of bubble sizes, a mutual approach within the calculated range does not invert the direction of the force.

From Fig. 5 it can also be seen that the important contributions for the net force come from the bubble wall motions before the first heavy collapse, because the afterbouncing results in fast oscillations that average to approximately zero. Thus the results should not strongly depend on the detailed

modeling of the collapse phase of motion. Indeed, qualitatively the same results have been obtained for isothermic compression of the gas ($\gamma=1$), for inclusion of a van der Waals hard-core term [29], and for the Gilmore model [30].

III. CONCLUSION

The mutual interaction forces between two small coupled gas bubbles ($R_0<10$ μm) in a strong low-frequency acoustic field ($P_a>1$ bar, $f=20$ kHz) have been investigated assuming that the spacing between the bubbles is large enough that the bubbles remain spherical for all times. The calculations have been carried out using Keller-Miksis equations which are mutual coupled by bubble pressure emission terms. Delay effects have been neglected.

For the considered parameter values a nonlinear resonancelike response of a single bubble occurs (dynamical Blake threshold). This leads to secondary Bjerknes forces between the bubbles that are stronger by a factor of 10^3-10^6 than expected from linear approximations in this driving frequency regime far below the bubbles' linear resonance frequency. Additionally, the signs of the forces change near the region of the dynamical Blake threshold. This result may be explained using the well-known linear resonance of the bubble as an analogy. If the bubbles both have radii larger (or smaller) than the resonance size, then they attract each other. If the resonance radius (where the response curve has a maximum) lies between the two bubble radii, then repulsion takes place. (In contrast to the linear resonance analogon, very small bubbles are again attracted by larger ones.) The boundaries of the such formed domains where repulsion occurs change with the driving amplitude, because the nonlinear resonance size of the bubble decreases with increasing pressure amplitude. The nonlinear resonance radius also depends on the distance of the bubbles, and increases when the bubbles approach each other. This in turn shifts the domain of the repulsion and changes the magnitude of the Bjerknes force, resulting in an overall shrinking of repelling regions. Only for some bubble pairs a mutual approach changes the sign of the force from attraction to repulsion, resulting in a stable separation distance. By far the most attracting bubbles in the considered parameter regime will approach further until nonspherical effects become important that are beyond the scope of this article.

Our findings are important for collective bubble phenomena in high-pressure fields such as streamer formation [5,31] and multibubble sonoluminescence [21], as linear modeling may lead to severe underestimation of the mutual bubble forces or to the wrong sign. In particular, secondary Bjerknes forces become comparable in size to primary Bjerknes forces (compare the values reported in Ref. [8]) even at considerably large bubble distances. Although a stable equilibrium distance between two violently oscillating bubbles is possible, stable static arrangements of more than two bubbles seem less likely because of the predominant attractive situations in parameter space. Indeed, streamer structures in strong acoustic fields incorporate dynamic arrangements of fast moving small bubbles [5,23], which is in contrast to static clusters of large bubbles in weak sound fields [32]. Future investigations will address to further details of coupled bubble oscillations in strong acoustic fields, for instance time retarded coupling and chaotic synchronization phenomena.

ACKNOWLEDGMENTS

This work was supported by the *Projektträgerschaft Internationales Büro*, the Ministry for Science, Higher Education and Technical Policy of the Russian Federation and the State Committee of the Russian Federation for Higher Education.

[1] V. F. K. Bjerknes, *Fields of Force* (Columbia University Press, New York, 1906).
[2] L. A. Crum, J. Acoust. Soc. Am. **57**, 1363 (1975).
[3] B. E. Noltingk and E. A. Neppiras, Proc. Phys. Soc. London Sect. B **63**, 674 (1950); E. A. Neppiras and B. E. Noltingk, *ibid.* **64**, 1032 (1951); H. G. Flynn, in *Physical Acoustics*, edited by W. P. Mason (Academic Press, New York, 1964), Vol. 1, p. 57.
[4] W. Lauterborn, Acustica **20**, 105 (1968).
[5] T. G. Leighton, *The Acoustic Bubble* (Academic, London, 1994).
[6] I. Akhatov, N. Gumerov, C. D. Ohl, U. Parlitz, and W. Lauterborn, Phys. Rev. Lett. **78**, 227 (1997).
[7] S. M. Cordry, Ph.D. thesis, University of Mississippi, 1995.
[8] I. Akhatov, R. Mettin, C. D. Ohl, U. Parlitz, and W. Lauterborn, Phys. Rev. E **55**, 3747 (1997).
[9] M. Kornfeld and L. Suvorov, J. Appl. Phys. **15**, 495 (1944).
[10] F. G. Blake, J. Acoust. Soc. Am. **21**, 551 (1949).
[11] M. D. Rosenberg, Technol. Memo Acoust. Res. Lab. Harvard Univ. **26** (1953).
[12] V. F. Kazantsev, Dokl. Akad. Nauk SSSR **129**, 64 (1959) [Sov. Phys. Dokl. **4**, 1250 (1960)].
[13] L. A. Crum and A. I. Eller, J. Acoust. Soc. Am. **48**, 181 (1969).
[14] G. N. Kuznetsov and I. E. Shchekin, Akust. Zh. **18**, 565 (1972) [Sov. Phys. Acoust. **18**, 466 (1973)].
[15] E. A. Zabolotskaya, Akust. Zh. **30**, 618 (1984) [Sov. Phys. Acoust. **30**, 365 (1984)].
[16] E. A. Zabolotskaya, Tr. Inst. Ob. Fiz. Akad. Nauk **18**, 121 (1989).
[17] A. A. Doinikov and S. T. Zavtrak, Phys. Fluids **34**, 94 (1995).
[18] H. N. Oguz and A. Prosperetti, J. Fluid Mech. **218**, 143 (1990).
[19] N. A. Pelekasis and J. A. Tsamopoulos, J. Fluid Mech. **254**, 501 (1993).
[20] M. Minnaert, Philos. Mag. **16**, 235 (1933).
[21] H. Kuttruff, Acustica **12**, 230 (1962); A. J. Walton and G. T. Reynolds, Adv. Phys. **33**, 595 (1984).
[22] S. Hilgenfeldt, D. Lohse, and M. P. Brenner, Phys. Fluids **8**, 2808 (1996).
[23] A. Billo, Ph.D. thesis, TH Darmstadt, Germany, 1996.
[24] R. I. Nigmatulin, I. Sh. Akhatov, N. K. Vakhitova, and R. T. Lahey, Jr., Dokl. Akad. Nauk. SSSR **348**, 768 (1996) [Sov. Phys. Dokl. **41**, 276 (1996)].

[25] R. I. Nigmatulin, I. Sh. Akhatov, N. K. Vakhitova, and R. T. Lahey (unpublished).
[26] J. B. Keller and M. Miksis, J. Acoust. Soc. Am. **68**, 628 (1980).
[27] A. Prosperetti and A. Lezzi, J. Fluid Mech. **186**, 457 (1986).
[28] U. Parlitz, V. Englisch, C. Scheffczyk, and W. Lauterborn, J. Acoust. Soc. Am. **88**, 1061 (1990).
[29] R. Löfstedt, B. P. Barber, and S. Putterman, Phys. Fluids A **5**, 2911 (1993).
[30] F. R. Gilmore, Report No. 26-4, Hydrodynamics Laboratory, California Institute of Technology, Pasadena, California, 1952.
[31] I. Akhatov, U. Parlitz, and W. Lauterborn, Phys. Rev. E **54**, 4990 (1996).
[32] A. A. Doinikov and S. T. Zavtrak, J. Acoust. Soc. Am. **99**, 3849 (1996).